International Tables for Crystallography (2006). Vol. F, Chapter 19.3, pp. 428–437.

19.3. Small-angle X-ray scattering

BY H. TSURUTA AND J. E. JOHNSON

19.3.1. Introduction

Mechanistic biology is frequently confronted with an experimental paradox. High-resolution structures are required to develop a chemical description of macromolecular interactions, but the processes themselves are dynamic and not amenable to high-resolution methods. Chemists and molecular biologists have been successful in generating homogeneous components and entire complex systems that are amenable to crystallization and high-resolution analysis. If the dynamics of the systems are small, as in the case of some enzymes and electron-transfer reactions, time-resolved studies can be performed in the context of the crystal lattice using Laue diffraction (Moffat, 1997; Genick *et al.*, 1997; Srajer *et al.*, 1996). If the dynamic features of the biological reactions are large, the motility must be studied in solution. During the last decade, small-angle X-ray scattering (SAXS) has emerged as an important method for studying large-scale dynamic processes, ranging from protein folding to virus particle polymorphism. The renaissance of this method has resulted from a variety of advances in molecular biology and X-ray instrumentation, and these have dramatically increased the information content of the derived results. Modern synchrotron X-ray sources and advanced detector systems have lead to higher-resolution data in both the spatial and time domains. Computational analyses of the data have improved dramatically, resulting, in some favourable cases, in *de novo* three-dimensional density functions from SAXS data that are comparable to a 20 Å-resolution electron-microscopy reconstruction. Model-based approaches to interpreting SAXS data have expanded their usefulness to the validation of mechanistic hypotheses involving movement or association of components independently determined at high resolution. Finally, SAXS studies have benefited from the same molecular-biology advances that provide large quantities of homogeneous material for crystallographic and NMR studies. The purpose of this chapter is to address practical aspects of SAXS as they relate to and complement macromolecular crystallography.

19.3.2. Small-angle single-crystal X-ray diffraction studies

We begin by briefly describing an obvious connection between small-angle solution X-ray scattering and single-crystal X-ray scattering, *i.e.* small-angle single-crystal diffraction (Tsuruta *et al.*, 1998; Miller *et al.*, 1999). The majority of macromolecular single-crystal studies ignore data at resolutions lower than 20 Å. Measuring these data accurately is generally difficult when collecting high-resolution data, because they are orders of magnitude stronger in intensity and frequently saturate the detector pixels or are intentionally blocked from reaching the detector by a large beam stop. It is technically challenging to record low-resolution data accurately, because they fall very close to the primary beam, where a variety of parasitic scattering effects occur. These data, however, contain information about the structure that may not be determined from only the high-resolution data. Low-resolution (∞–15 Å) data are sensitive to structures that are organized over large distances and that contribute primarily to the low-frequency terms in a Fourier series. In contrast, portions of the structure that contribute to high-frequency terms must be in precisely the same position in all the unit cells within the crystal. Two examples illustrate the importance of low-resolution terms.

Assume that an exposed loop on the surface of a protein is highly mobile. The scattering-factor curves for atoms in this loop will be highly attenuated by the large Debye–Waller factor. If the temperature factors are high enough, these atoms will contribute nothing to the high-resolution data. In contrast, these atoms will contribute strongly to the low-resolution data. If the low-resolution terms are included in the Fourier series, the atom positions will not appear as individual atoms; instead, an envelope of density describing the statistically distributed positions of these atoms will be visible, and this can aid significantly in the modelling of the loop.

A second example is the nucleic acid within a spherical virus. The nucleotides generally do not display the symmetry of the icosahedral capsid, although in some cases segments of RNA or DNA clearly interact with the protein and are therefore visible at high resolution. The RNA density is not usually visible if only higher-resolution data are used, and the virus particle appears empty. The reason for this is that the RNA is best described as a uniform sphere within the particle, and the Fourier transform of such a sphere falls off rapidly if the sphere is relatively large. A typical RNA virus will have an internal RNA core of about 100 Å in radius. The scattering contribution of this region is virtually zero beyond 20 Å resolution. If the low-resolution data are measured accurately, the region occupied by RNA and its general level of interaction with the coat protein can be clearly seen (Fig. 19.3.2.1).

The relation between single-crystal and solution X-ray scattering is clearly illustrated in Fig. 19.3.2.2, where the scattering of a single crystal and the solution scattering of a 320 Å-diameter RNA virus are compared. The figure shows the scattering expected for a uniform sphere 160 Å in radius, the observed solution X-ray scattering from this virus and the single-crystal diffraction from

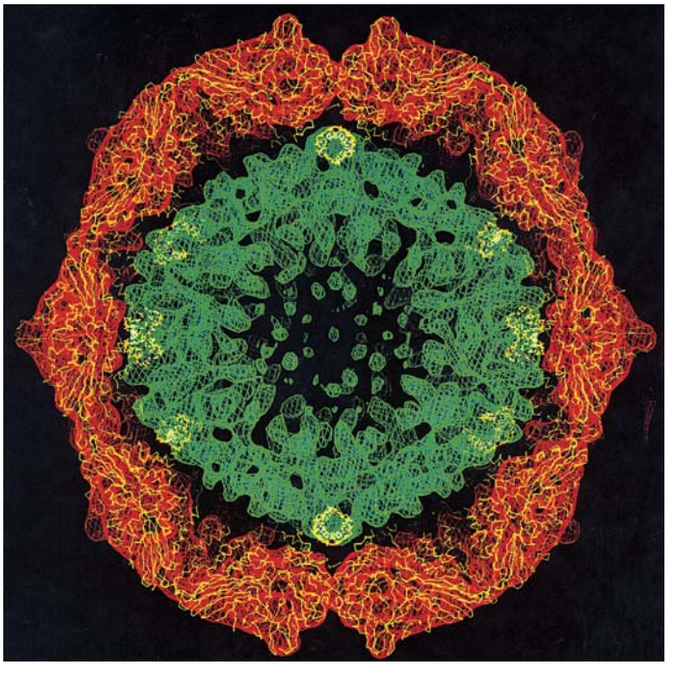

Fig. 19.3.2.1. A cross section of the electron-density map of sFHV at 14 Å resolution. The density shown in red corresponds to the protein capsid, while density in green corresponds to the bulk RNA or dynamic protein segments. The Cα backbone of the atomic model of the protein capsid seen in the high-resolution structures of sFHV is shown as yellow traces, and the model of the ordered pieces of duplex RNA is shown as a stick model. The high-resolution protein model fits the electron-density map very well. The ordered RNA model is buried in the RNA density in green.

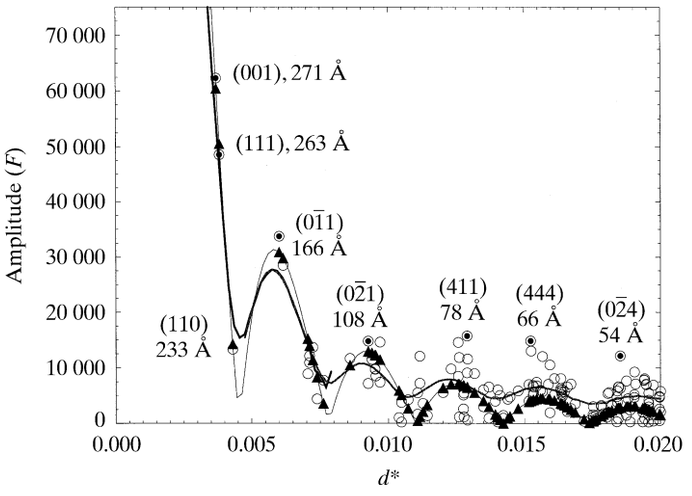

Fig. 19.3.2.2. Comparison of the absolute values of single-crystal reflection amplitudes (circles), the solution scattering intensity (thick curve) and the calculated scattering intensity from a uniform sphere (thin curve).

the virus. All three diffraction patterns are in close agreement at resolutions below 50 Å, with the only difference being the continuous sampling of the transform in the computed and solution scattering curve and the discrete sampled transform of the crystalline virus. The RNA density in Flock house virus (FHV) shown in Fig. 19.3.2.1 illustrates the information content of the low-resolution data. DNA density functions in polyoma virus were mapped by employing similar methods (Griffith *et al.*, 1992). Low-resolution single-crystal data are also critical for applying the methods of *de novo* phase determination. Geometric solids, such as a sphere, or a low-resolution electron cryo-microscopy (cryoEM) reconstruction may serve as initial phasing models for such a strategy, and the procedure of refining and extending phases is much more robust if the low-resolution data are measured accurately (Tsuruta *et al.*, 1998).

19.3.3. Solution X-ray scattering studies

Protein crystals have high solvent content: typically 50% and as much as 80% in some cases (*e.g.* Johnson & Hollingshead, 1981; Wikoff *et al.*, 1998). Some solvent is well ordered and visible in the crystal structure. Some, referred to as bulk solvent, is dynamic, not specifically associated with parts of the repetitive lattice and can be readily exchanged within the crystal using a flow cell. The high solvent content of macromolecular crystals makes it probable that most of the features of a protein molecule that are important for its function in solution are preserved in the crystallographic structure. Cases are known, however, in which lattice forces or crystallization conditions have masked functional features of the macromolecule or induced functionally irrelevant oligomerization. A straightforward application of solution scattering is the verification of the relevance of the oligomerization state of a macromolecule observed in the crystal. The methods are complementary, because the crystal structure almost invariably leads to the correct secondary and tertiary structures for the monomer, and the SAXS experiment allows the determination of the quaternary structure of the macromolecule in solution.

The solution scattering pattern of the macromolecule can be calculated directly from a set of atomic coordinates. Scattering computed from models of different oligomerization states or from models of the monomer can be readily compared with the observed scattering pattern. In many cases, not only can the oligomer state be determined, but also the point-group symmetry of the oligomer; hence more information is available than through a solution molecular-mass determination by other physical methods. Using the same approach, effects of various ligands on the state of a protein can be studied in solution. Any large-scale structure alteration of a protein, including changes in quaternary structure or folding and unfolding, can be readily studied in solution, either as a static experiment or as a time-resolved investigation.

Recently, the search for crystallization conditions of macromolecules has been refined by the use of dynamic light scattering. Solution X-ray scattering can be even more effective because it is sensitive to molecular aggregates that are smaller than those detected by light scattering, and this broadens the radius of convergence for conditions that will produce good-quality crystals. For example, the interparticle interaction potential of proteins with a mass of less than 100 kDa can be readily measured in the SAXS experiment, and this has been shown to be an important factor in their crystallization (Bonneté *et al.*, 1997). In a particularly successful experiment, a set of small-angle solution X-ray scattering results was used to improve crystallization conditions, and this lead to single crystals that diffracted beyond 1.9 Å (Mourey *et al.*, 1997). A similar approach was used to distinguish between virus coat protein polymerization and crystallization (Petitpas *et al.*, 1998). Studies in which a number of solution conditions must be tested can be done most effectively using synchrotron small-angle scattering facilities, though it is possible to conduct such studies with a conventional X-ray source.

19.3.3.1. *Information content of solution scattering*

Solution scattering deals with samples that are randomly oriented in a solvent. Three-dimensional information is compressed to one dimension, and a one-dimensional self-correlation function (a rotationally averaged Patterson function) of the protein is obtained when the scattering function is properly Fourier transformed. Excellent books describing the information content of small-angle scattering include those by Guinier & Fournet (1955) and Glatter & Kratky (1982), and for modern perspectives see Feigin & Svergun (1987). Concise reviews with a strong focus on structural biology have also appeared, including those by Trewhella (1998) and Koch (1991). These reviews describe the theoretical background, experimental considerations and ways of extracting structural information. None of these take our perspective, which is addressed to the sceptical crystallographer.

Assume a monodisperse protein solution. X-ray scattering from the solution originates from the excess electron density of protein particles over that of the solvent, $\Delta\rho(\mathbf{r}) = \rho(\mathbf{r})_{\rm protein} - \rho_{\rm solvent}$ (Fig. 19.3.3.1). Note that $\rho(\mathbf{r})_{\rm protein}$ is typically only about 30% higher than $\rho_{\rm solvent}$, and that $\Delta\rho(\mathbf{r})$, the electron-density 'contrast', depends on the solvent composition. The scattering intensity observed for such a system is given by

$$\begin{aligned} I(Q) &= F(Q)F^*(Q) \\ &= \int_{\mathbf{r}_1\mathbf{r}_2} \Delta\rho(\mathbf{r}_1)\Delta\rho(\mathbf{r}_2)\exp[-iQ(\mathbf{r}_1-\mathbf{r}_2)]\,{\rm d}V_1\,{\rm d}V_2, \quad (19.3.3.1)\end{aligned}$$

where $Q = 4\pi\sin\theta/\lambda$ (2θ is the scattering angle and λ is the wavelength of the X-radiation used). Owing to the rotationally averaged nature of solution scattering, the exponential term may be substituted with the Debye function, $(\sin Q\mathbf{r})/Q\mathbf{r}$, giving

$$I(Q) = \int_{\mathbf{r}} 4\pi\mathbf{r}^2\Delta\rho(\mathbf{r})^2(\sin Q\mathbf{r})/Q\mathbf{r}\,{\rm d}\mathbf{r}. \quad (19.3.3.2)$$

Guinier & Fournet (1955) showed that equation (19.3.3.2) can be approximated by a Gaussian function at relatively small scattering angles resulting in

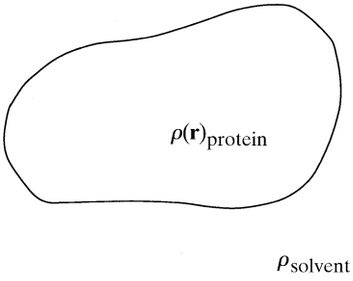

Fig. 19.3.3.1. Definition of electron-density contrast. The excess electron density of protein particles over that of the solvent, $\Delta\rho(\mathbf{r}) = \rho(\mathbf{r})_{\text{protein}} - \rho_{\text{solvent}}$, is the origin of solution X-ray scattering.

$$I(Q) = I(Q=0)\exp(-Q^2R_g^2/3). \qquad (19.3.3.3)$$

This approximation is theoretically valid for $Q \leq 1/R$. Physical parameters of the system that can be determined from the solution scattering experiment are R_g, the radius of gyration of the molecule and $I(Q=0)$, the scattering intensity at zero angle. The radius of gyration is defined as the root-mean square of the distances of all electrons from their centre of gravity. The radius of gyration can be related to characteristic dimensions of relatively simple objects. For instance, $R_g^2 = (3/5)R^2$ for a sphere of radius R, and $R_g^2 = (a^2 + b^2 + c^2)/5$ for an ellipsoid with semi-axes a, b and c (Feigin & Svergun, 1987). The scattered intensity at zero angle is proportional to the square of the molecular mass of the macromolecule at a defined number concentration. A plot of $\ln I(Q)$ *versus* Q^2 is called a Guinier plot, and if the system is monodisperse and the macromolecule is relatively globular in shape, the plot will be linear up to at least $Q_{\max} = 1/R_g$ (Fig. 19.3.3.2*a* inset). The Guinier plot should begin at a Q value significantly smaller than $1/R_g$. In practice, many investigators take the Q range for the plot to higher Q values such as $Q_{\max} = 1.5/R_g$, or nearly to $2.0/R_g$, since the Guinier plot is often linear to higher Q values. Significant deviation from linearity in the Guinier region is an indication of polydispersity or an extreme deviation from globular shape, such as a cylinder. The solution scattering intensity is proportional to the molecular mass of a particle, thus it is very sensitive to the presence of even a trace amount of large oligomers. Discrete oligomeric states can be identified by the electron pair distance correlation functions as shown in Fig. 19.3.3.2(*b*). A second contribution to nonlinear Guinier plots is interparticle interference due to strong interactions among particles. In these cases, the particle correlation function is overlaid on the scattering function from the molecular envelope. Strong interparticle interference is illustrated in the example in Fig. 19.3.3.3. The P0 glycoprotein was solubilized with sodium dodecyl sulfate (SDS), whose net charge expels solubilized protein particles from each other, generating a correlated interparticle distance in the range of 250 Å. While the correlation is rather weak at 2 mg ml^{-1}, much stronger interference is seen at higher concentrations. This is an extreme example of interparticle interference, because a noticeable interference peak is observed in a much higher concentration range, well over 10 mg ml^{-1}, for most soluble proteins. Smaller proteins often exhibit more pronounced interparticle interference at lower concentrations than larger proteins, perhaps because the number concentration of protein molecules is higher with smaller proteins. In the case of the 100 kDa protein in Fig. 19.3.3.3(*b*), no detectable interference peak is seen. While Guinier plots are linear throughout the concentration range studied, the slope, *i.e.*, the radius of gyration, gradually decreases as the protein concentration is increased (data not shown). Also note that a small inorganic molecule could change the interparticle interference, as seen in slight change in the slope of the R_g *versus*

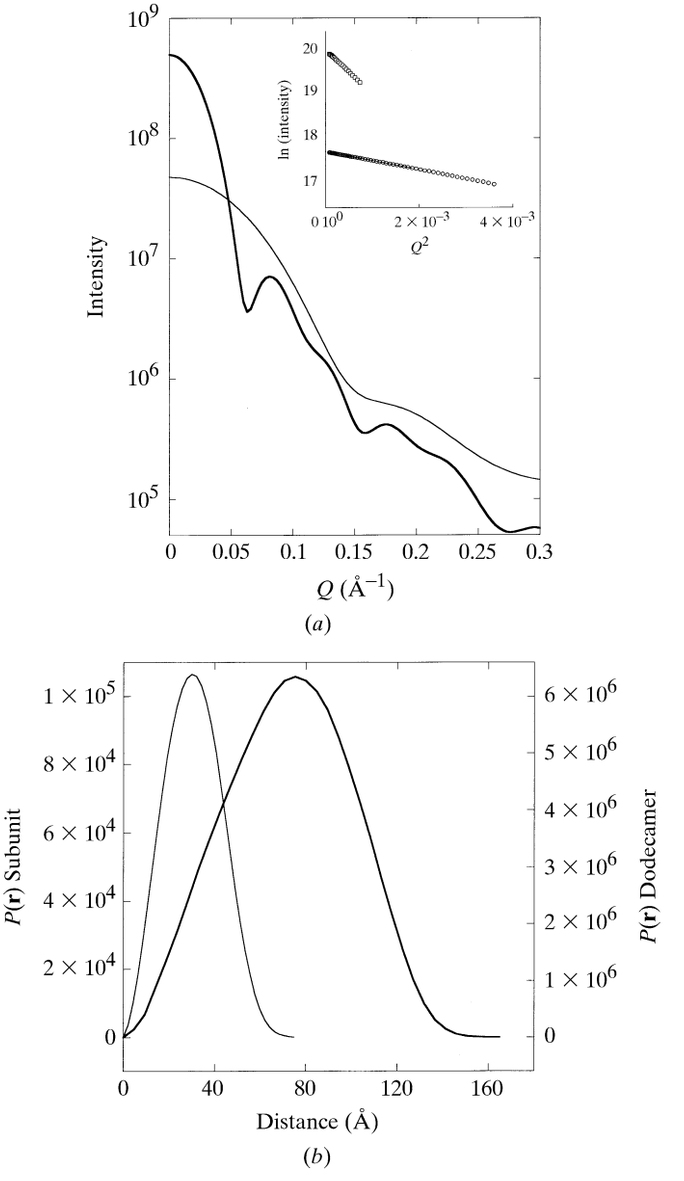

Fig. 19.3.3.2. (*a*) The calculated solution X-ray scattering curves from the crystal structure of *Salmonella typhimorium* glutamine synthetase. Glutamine synthetase is composed of 12 identical 469-residue subunits and forms a functional dodecameric assembly (PDB entry 2GLS; Yamashita *et al.*, 1989). The single subunit was computationally isolated, and the solution scattering curves for the subunit (thin line) and the assembled form (thick line) were calculated with a 3 Å-thick hydration layer of 0.03 e Å^{-3} using *CRYSOL* (Svergun *et al.*, 1995). The curves are normalized to an identical weight concentration, that is, the number concentration of the dodecamer is 1/12 of that of the subunit, giving a 12-fold increase in $I(Q=0)$. The inset shows Guinier plots of the calculated scattering curves. The radii of gyration determined by the Guinier plot to $Q \simeq 1.0/R_g$ (solid-line fit) for the subunit and the assembled form are 24.1 and 55.8 Å, respectively. The 'extended' Guinier plots to $Q \simeq 2.0/R_g$ (circles) give 23.9 and 56.5 Å. Note that both Guinier plots are quite linear beyond $Q \simeq 2.0/R_g$, although the Guinier approximation is theoretically valid to $Q \simeq 1.0/R_g$. It should be noted, however, that the 'extended' Guinier plot tends to give significantly smaller R_g for elongated shapes. (*b*) The electron distance distribution functions. The pair distribution functions $P(\mathbf{r})$ were calculated from the scattering curves in (*a*) using *GNOM* (Svergun, 1992). The maximum intramolecular distance is 75 and 160 Å for the subunit and the assembled enzyme, respectively. The $P(\mathbf{r})$ gives the radius of gyration as 23.6 Å for the subunit and 55.0 Å for the assembled enzyme.

concentration plot. This small ligand induces a conformational change in the protein, which alters its electrostatic properties. The best results are usually obtained when scattering curves are recorded at a few different protein concentrations and then extrapolated to infinite dilution. This procedure generates a scattering curve free from interparticle interference. Extrapolated values of R_g are often used to assess the magnitude of protein conformational changes. The interparticle interference, on the other hand, could be used to evaluate electrostatic properties of the protein, though this effect has not yet been clearly linked to any specific physical parameter, except the second virial constant. Note that the positive slope of the R_g *versus* concentration plot is an indication of either concentration-dependent oligomerization or non-specific aggregation. Different solution conditions should be tested to avoid a positive slope. The forward scattering intensity $I(0)$ is calculated by extrapolating the Guinier plot to $Q = 0$. $I(0)$ is proportional to the number of electrons in a particle, though it depends on the solvent electron density, given the definition of electron-density contrast. This complicates the determination of absolute molecular weight. Relating the measured $I(0)$ values to the molecular mass of the protein thus requires a well characterized monodisperse protein system with a known molecular weight for calibration. A solution of hen egg lysozyme or bovine serum albumin is often used. These proteins, however, tend to show significant changes in scattering intensity at very small angles due to radiation-induced aggregation under a full synchrotron-radiation beam. Synthetic polymers such as polyethylene are convenient standards because of their high stability; however, they scatter X-rays orders of magnitude more than many protein solutions, making it difficult to scale the data to such a standard. The problem is not usually serious, as most biological studies deal with proteins of known molecular mass. Studies of oligomeric proteins are simplified, because a species of known molecular mass, *e.g.*, a monomer, usually serves as an internal standard. The Guinier plot ln $I(Q)$ *versus* Q^2 is no longer linear, even at small angles, when the shape of the protein deviates significantly from a globular shape. A plot of ln $QI(Q)$ *versus* Q^2 gives a radius of gyration of the cross section and mass per unit length for a rod-like particle as well as a radius of gyration of thickness and mass per unit area (Feigin & Svergun, 1987; Glatter & Kratky, 1982).

Other information obtained directly from the experiment when there is no *a priori* knowledge of the structure is the electron pair distribution function $P(\mathbf{r})$, *i.e.*, the histogram of distances of all possible pairs of electrons within a particle (Fig. 19.3.3.4). This quantity is obtained from the Fourier transform of the observed scattering intensities. Fourier termination effects and smearing of scattering curves due to the use of a nonideal experimental geometry must be considered in the derived result. Algorithms have been developed to incorporate the experimental geometry in the back Fourier transform (Glatter, 1999; Moore, 1980). The use of nearly parallel, focused synchrotron X-ray beams, with a small beam cross section and a long sample-to-detector distance, often eliminates the need for desmearing scattering curves and this leads to $P(\mathbf{r})$ functions with minimal errors from data correction and manipulation. $P(\mathbf{r})$, in turn, gives R_g and $I(Q = 0)$:

$$R_g = (1/2) \int^{D_{\max}} \mathbf{r}^2 P(\mathbf{r})\, \mathrm{d}\mathbf{r} \Big/ \left(\int^{D_{\max}} P(\mathbf{r})\, \mathrm{d}\mathbf{r} \right), \qquad (19.3.3.4)$$

$$I(0) = 4\pi \int^{D_{\max}} P(\mathbf{r})\, \mathrm{d}\mathbf{r}. \qquad (19.3.3.5)$$

The entire scattering curve is used to obtain $P(\mathbf{r})$, thus giving more accurate values for R_g and $I(0)$ than those from a Guinier plot, even when the data do not cover many of the scattering angles below $Q = 1/R_g$. The values of R_g obtained from $P(\mathbf{r})$ tend to be less sensitive to trace amounts of contaminating higher aggregates.

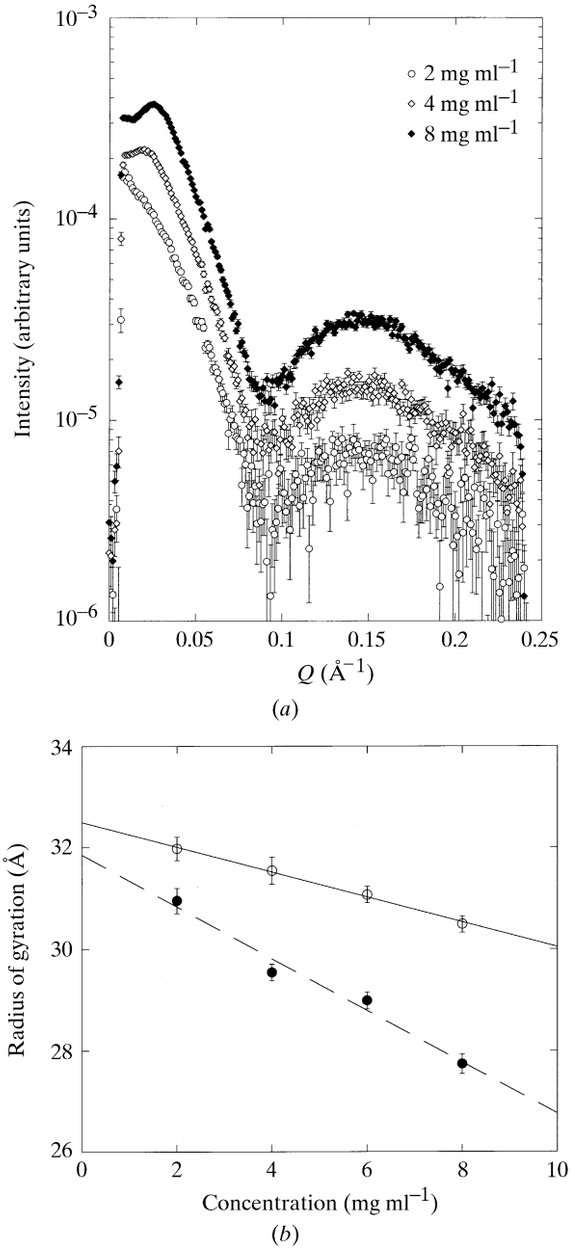

Fig. 19.3.3.3. (*a*). Interparticle interference in biological small-angle scattering. Scattering from myelin P0 glycoprotein solubilized in 0.1% SDS, recorded at 2, 4 and 8 mg ml^{-1} (Inouye *et al.*, 1999). (*b*) Plots of measured radii of gyration of *E. coli* aspartate transcarbamoylase catalytic trimer *versus* concentration in the absence (open circles) and presence (filled circles) of the bisubstrate analogue *N*-phosphoneacetyl-L-aspartate (E. R. Johnson, H. Tsuruta & H. K. Schachman, unpublished data).

19.3.3.1.1. *Solution scattering and crystal structures*

SAXS is an extremely powerful method for studying the relative change in molecular weight, and thus the oligomerization state, of a protein system. Such studies are useful in the case of proteins that change in quaternary structure as a means of regulating biological function. Changes in association state such as $n\mathrm{A} \leftrightarrow \mathrm{A}_n$ lead to a large change in $I(0)$, which is proportional to the square of the molecular mass and to the number of particles in solution. In the example illustrated in Fig. 19.3.3.2, the formation of a dodecameric assembly composed of 12 identical subunits at a constant weight concentration results in the increase in $I(0)$ by a factor of 12.

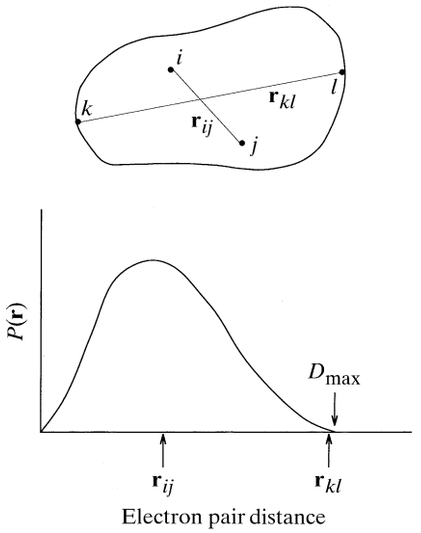

Fig. 19.3.3.4. Definition of the electron pair distance distribution function $P(\mathbf{r})$. It is a histogram of all electron pair distances within a particle as depicted here. The largest dimension of the molecule $D_{\max}$ is determined from the point where $P(\mathbf{r})$ falls to zero.

The radius of gyration can be readily calculated with atomic coordinates, employing a program such as *X-PLOR*. This provides a quick means of verifying the overall crystal structure in solution. R_g values measured in solution are often larger, by up to a few ångstroms, than those calculated from atomic coordinates. Such differences are larger than statistical errors in a carefully planned set of experiments, although trace amounts of molecular aggregates due to the presence of naturally present higher oligomers, impurities or radiation-induced aggregation could increase apparent radii of gyration. The apparent protein envelope may be enlarged significantly by the presence of structured water molecules surrounding the protein. Strongly associated water molecules on the protein surface are significant, because the electron-density contrast between a protein and a solvent is small (Lattman, 1989). A recent study by Svergun, Richards *et al.* (1998), combining X-ray and neutron solution scattering techniques, verified that the hydration layer is critical when interpreting solution X-ray scattering curves based on crystal structures, because crystallographic structures underestimate the extent of the hydration layer. This layer is about 3 Å thick, with an average density about 10% higher than that of bulk solvent. The program *CRYSOL*, developed by Svergun *et al.* (1995), has incorporated the first hydration layer in the calculation of scattering curves and radii of gyration, providing estimates of the scattering close to those observed experimentally.

The Debye formula, (19.3.3.6) below, demonstrates that solution scattering intensity is sensitive to the overall shape of the molecule and can readily follow changes in particle dimensions. The intensity of scattering is given by

$$I(Q) = \sum_i \sum_j \Delta\rho(\mathbf{r}_i)\Delta\rho(\mathbf{r}_j)\sin[Q(\mathbf{r}_i - \mathbf{r}_j)]/Q(\mathbf{r}_i - \mathbf{r}_j), \quad (19.3.3.6)$$

where the indices represent individual mass elements or electrons. The solution scattering intensity from a macromolecule of known structure can be calculated readily with this expression. An entire scattering curve can be computed rapidly, even for molecules with thousands of atoms. For instance, calculation of the scattering curve of a glutamine synthetase subunit with 3636 atomic positions took approximately 30 min with a DEC Alpha workstation. The calculation of the dodecameric assembly of glutamine synthethase was performed using only α-carbon positions, instead of all atomic positions, to reduce computation time. This approach still approximates the molecular envelope of this large molecular complex very well, and the effect of the hydration layer could be incorporated, as proposed by Lattman (1989). Alternatively, three-dimensional objects can be approximated by a sum of spherical harmonics (Harrison, 1969; Stuhrmann, 1970), and the Fourier transform of the spherical harmonic expansion is an effective method for evaluating the Debye formula. The program *CRYSOL*, developed by Svergun *et al.* (1995), can compute the entire scattering curve for the dodecameric glutamine synthetase in 10 min using this method. Explicit incorporation of symmetry allows a solution scattering curve from giant molecular complexes, such as an icosahedral virus particle, to be computed efficiently (Zheng *et al.*, 1995).

19.3.3.1.2. *Low-resolution model determination using solution scattering*

The coordinates for a structure are often unavailable, but its general shape is known from electron microscopy or hydrodynamic studies. Pilz *et al.* (1979) demonstrated that reasonable scattering patterns from complex systems could be generated using a model that approximated the shape of a large complex with a number of uniform-density spheres. This approach has been improved over the years to make it less dependent on initial models. For instance, a genetic algorithm was recently used to select a few best models composed of uniform-density spheres to generate density functions in close agreement with solution scattering data (Chacón *et al.*, 1998). A program for this approach, *DALAI_GA*, has recently been released. There have been other effective approaches to the determination of low-resolution structures from solution scattering, including Monte Carlo methods (Olah *et al.*, 1995) to select the most plausible model among many possibilities. On the other hand, the program *DAMMIN* uses simulated annealing for optimization (Svergun, 1999).

Multiple-sphere modelling approaches involve many parameters, and the verification of resulting models can be difficult. This is a fundamental problem in solution scattering, because random orientation of a protein in solution limits the number of structural parameters that can be determined reliably. The scattering curve recorded in the resolution range 700 to 20 Å, a typical angular range covered in solution X-ray scattering studies of proteins, allows only a small number of parameters to be refined, typically less than 20, according to Shannon's information theorem. Density functions for oligomeric proteins displaying specific molecular symmetry can be computed directly from the solution scattering pattern with spherical harmonic expansions that reflect the symmetry (Jack & Harrison, 1975). A set of solution scattering curves from components of an icosahedral virus particle (Schmidt *et al.*, 1983) was analysed by an icosahedral harmonic expansion technique, directly generating a low-resolution structure of the virus particle that was comparable to one determined by cryo-electron microscopy and image reconstruction (Zheng *et al.*, 1995). More recently, density functions for asymmetric particles were derived *de novo* from the solution scattering patterns with a spherical harmonic expansion and no imposed symmetry (Svergun *et al.*, 1996). An interactive modelling tool has been developed that combines the spherical harmonics approach with placement of protein-subunit coordinates in real space to construct a model for a large macromolecular complex using solution scattering data (Kozin *et al.*, 1997).

19.3.3.2. *Instrumentation for small-angle X-ray scattering*

A small-angle X-ray scattering instrument typically consists of an X-ray source, a set of X-ray optics, a sample holder and a

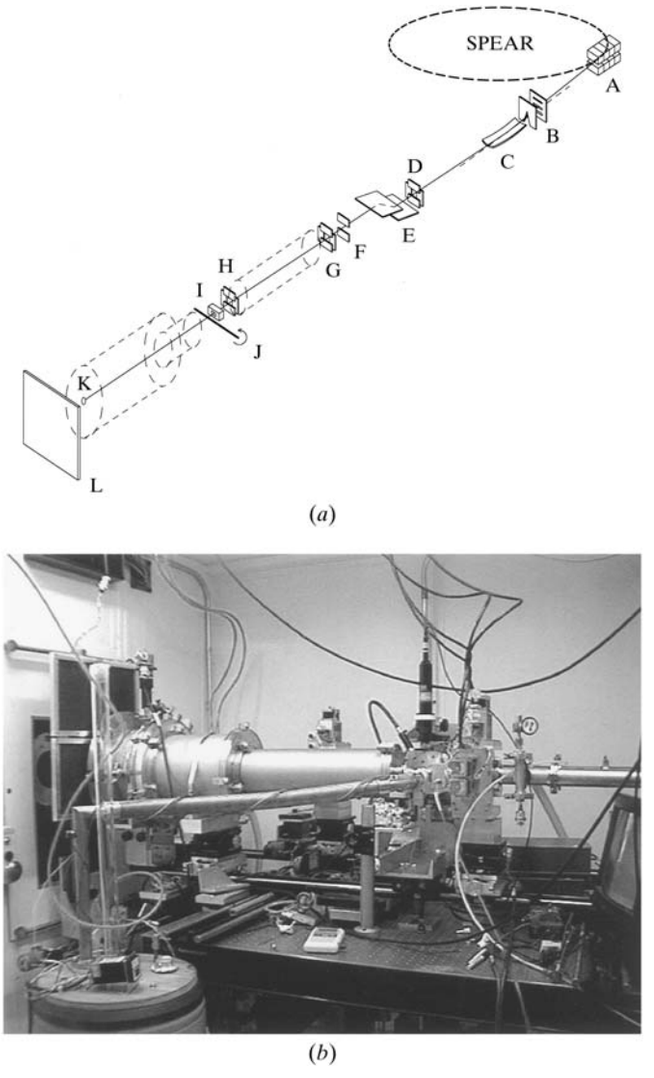

(*a*)

(*b*)

Fig. 19.3.3.5. A small-angle X-ray scattering instrument on BL 4-2 at the Stanford Synchrotron Radiation Laboratory. (*a*) A diagram of the instrument composed of an eight-pole wiggler source (A), mirror slits (B), toroidal focusing mirror (C), monochromator slit (D), double-crystal monochromator (E), fast beam shutter (F), beam-defining slit (G), guard slit (H), ion chamber (I), crystal spindle axis (J), which would be replaced with a solution sample cell for solution X-ray scattering, beam stop (K) and an image plate detector (L), which would be replaced with a gas-chamber detector for solution scattering. Vacuum beam flight paths are drawn in dotted lines. (*b*) A view of the instrument as configured for small-angle single-crystal diffraction with a crystal-to-detector distance of 1.3 m. Some of the components in (*a*) are also seen in (*b*).

detector system (Fig. 19.3.3.5). The source can be an X-ray tube, a rotating-anode source or synchrotron radiation. The choice of optical components depends on the type of source, beam-flux requirement and angular range to be covered. The optics system includes a beam focusing device, such as a mirror, a monochromator, beam-collimation slits, vacuum paths and a beam stop. Owing to the very weak level of X-ray scattering from solutions of biological macromolecules, caution must be taken to minimize scattering from air and window materials used in the sample holder as well as to contain elements of the system under vacuum. The choice of detector depends primarily on the level of signal expected for typical samples at the detection plane. Other factors that are crucial in choosing a detector system include active area, spatial resolution and read-out speed. The level of noise generated within an entire detector system must always be constant and preferably much lower than the weakest level of signal to be measured.

19.3.3.2.1. *Instruments on conventional sources*

Kratky cameras, which are commercially available, have been used for many years in small-angle X-ray scattering studies of synthetic polymers and relatively large biological systems (Glatter & Kratky, 1982). These instruments record scattering in only one dimension, thus they are not always suitable for the study of weak X-ray scatterers, although excellent accessibility to small angles is often achieved. More recent small-angle X-ray scattering instruments have a pinhole collimation system similar to those used on synchrotron instruments described below. They allow isotropic scattering to be measured with a two-dimensional detector (Bu *et al.*, 1998). Synthetic multilayered materials, such as Mo-B_4C, formed on a figured surface serve as a monochromator element as well as a focusing device and produce an X-ray beam with very small divergence (Schuster & Göbel, 1995). Many instruments on conventional sources could benefit from this new development in X-ray optics.

19.3.3.2.2. *Synchrotron instruments*

The needs for time-resolved capability and for measuring weak X-ray scattering have lead to the development of synchrotron small-angle X-ray scattering instruments. Most of these instruments employ the pinhole camera geometry and are suitable for fibre diffraction experiments as well. [For a review, see Koch (1988).] Major synchrotron facilities that produce radiation in the hard X-ray regime have at least one small-angle X-ray scattering instrument of this type. Gas proportional counters are common with these instruments, as they allow photon counting virtually without added noise (Petrascu *et al.*, 1998). Gas proportional counters are equipped with very fast electronics modules, allowing more than 1000 time-resolved scattering patterns to be recorded successively every second (Boulin *et al.*, 1988). The disadvantage of these detectors is the count-rate limit, *i.e.*, counting efficiency drops to below 50% at about 10^5 to 10^6 counts per second. This is due to the fact that the position of photon arrival is converted to a time domain, which is then registered in a histogram memory module. The space-to-time conversion occurs first on the delay lines incorporated in the gas-chamber detector, then the time-to-space conversion is performed by time-to-digital converters. These processes take a fraction of a μs per X-ray photon using present technologies. The position of the X-ray photon cannot be recorded effectively when another photon is being processed, thus leading to the count-rate problem mentioned above. Cipriani *et al.* (1994) proposed a new delay-line technology to increase this limit by a factor of at least 10, making gas-chamber detectors useful at high count rates. Experimenters should, however, be aware of space-charge effects in gas proportional counters. Two experimental artifacts can be observed. First, intensity near the beam stop is reduced when macromolecular complexes are studied. Second, peaks with high intensity can be reduced at their maximum, giving the impression of two closely spaced weaker peaks with a trough at the location of the true peak. Arriving photons are not counted by the detector when the local count rate exceeds the recombination rate of a detector gas molecule. Modern integration detectors, such as the image plate and the charge-coupled-device (CCD)-based detectors, have virtually no count-rate limit and have been characterized for small-angle scattering. These new detectors have certain limitations, such as a relatively slow data-acquisition rate, a problem for time-resolved studies. In general, care should be taken to match the detector to the experiment.

19.3.3.3. *Experimental considerations*

19.3.3.3.1. *Sample preparation*

Sample volumes required for one measurement are between 10 to 50 µl, occasionally more, depending on the specific design of the sample cell used. The concentration required to record a scattering curve with satisfactory statistics depends primarily on the molecular weight of the protein and the beam flux. Approximately 1 mg ml^{-1} of a small protein (10–20 kDa) is the lower limit for recording a scattering pattern with satisfactory statistics when experiments are performed with a typical synchrotron instrument equipped with a gas-chamber detector. Somewhat lower concentrations of larger molecular weight proteins may be used. Higher concentrations will improve statistics significantly and reduce exposure times, but interparticle interference may result from high concentrations. Time-resolved experiments benefit dramatically from higher sample concentrations. In addition to the scattering power of the sample, the signal-to-background ratio and overall stability of an instrument (from X-ray source and optics to detector) limit the lowest concentration for a given experiment. Although higher concentrations add dramatically to the scattering and improve statistics, sample solutions must be monodisperse. Small-angle solution scattering is not well suited to the study of polydisperse systems, which give scattering of the entire molecular population weighted by the square of the mass, although a few distinct populations of substantially different sizes may be resolved with good-quality data. Chemical components that may have been carried along in a sample preparation, such as ammonium sulfate, sucrose, chloroform or caesium chloride, should be removed. The presence of such compounds may change the electron-density contrast and X-ray absorbency of the sample. In general, this can be most effectively avoided by exhaustive dialysis with the desired buffer solutions. The outer solution used for the final dialysis should be used for the blank measurements. Scattering contributions from the buffer solution, the sample cell and parasitic scattering must be subtracted from the measured scattering curve; these can be measured accurately from a well prepared blank. Extra buffer solution should be available for sample dilution. The data quality is improved and problems with radiation-sensitive samples are readily detected when protein concentrations and biological activities of samples are measured before and after the scattering experiment. Accurate protein concentration measurements permit scattering intensities from different samples to be scaled together accurately. This is particularly important in determining molecular weight.

19.3.3.3.2. *Sample-handling devices*

Sample holders used in solution scattering are either Lindeman glass or quartz capillaries, or machined cells equipped with flat windows (Fig. 19.3.3.6). Glass capillaries have been widely used to contain a sample solution. A beam size significantly smaller than the diameter of the capillary is required to minimize strong parasitic scattering from the round edge of the capillary. A large beam size in the horizontal direction may be used with capillaries to obtain stronger scattering intensity without adding parasitic background. Capillary cells are suitable for measuring scattering primarily in the direction perpendicular to the long axis of the cell. The advantage of the capillary cell is the small volume of sample solution required for measurements. About 4 µl of a sample solution in a 1 mm-diameter capillary provides sufficient material for the experiment. By employing a specialized holder, a capillary cell can be placed under a vacuum, minimizing air scattering (Dubuisson *et al.*, 1997). This feature is useful for solution scattering studies of small proteins. Anaerobic samples may be sealed in a capillary.

Another common sample cell holds the solution between a pair of flat windows. This cell offers two improvements over capillary cells – a larger beam cross section may be used, which increases the number of photons incident on the sample, and a two-dimensional detector can be effectively used for recording the scattering. Flat-window cells are available that require only about 10 µl of solution. Both capillary and flat-window cells require a holder with temperature regulation. The choice of window materials for the sample container is important because of the weak sample scattering. An X-ray-transparent material is required that has little intrinsic scattering within the scattering-angle range of the sample. Common window materials include synthetic mica of high purity and certain types of polypropylene and polyamide. Etched high-

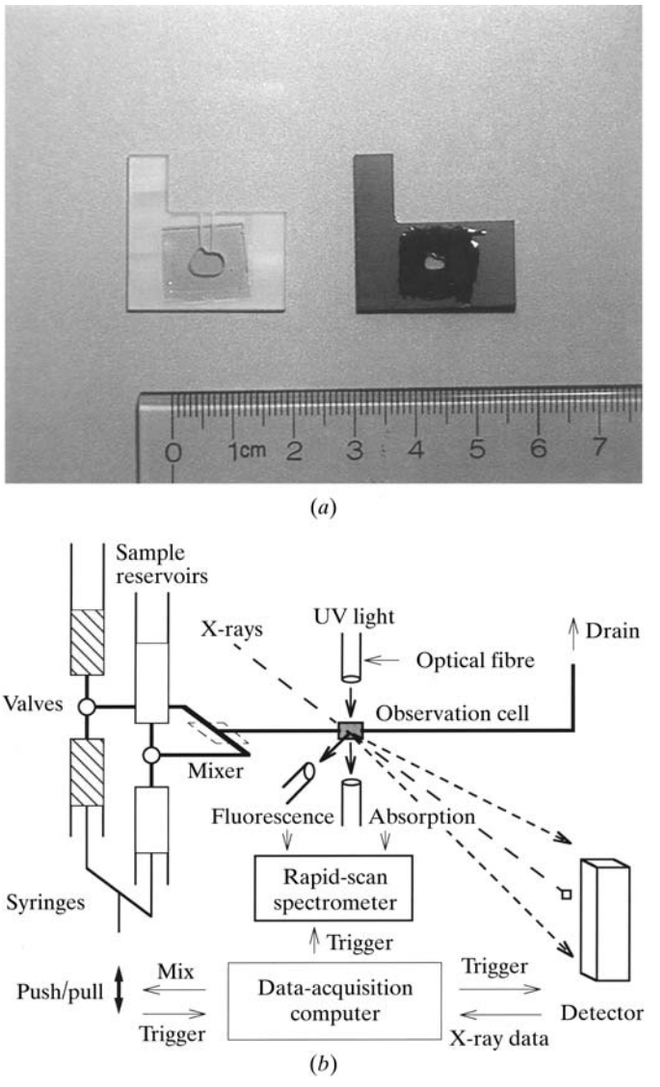

Fig. 19.3.3.6. (*a*) Flat-window cells for solution scattering and (*b*) a diagram of a stopped-flow rapid mixer for time-resolved solution scattering. The solution cell to the left in (*a*) is made of polycarbonate and is equipped with two synthetic mica windows. A sample solution is injected through one of two sample loading channels using a microsyringe. The black cell to the right is made of coloured polyoxymethylene for light-activated, time-resolved studies and has a smaller sample chamber. In (*b*), two solutions, *e.g.* an enzyme solution and a substrate solution, are put in sample reservoirs, loaded into individual syringes and wait for a trigger signal from the data-acquisition system. Then the two solutions are rapidly mixed, transferred to the observation cell, typically within 5 ms or less, and a trigger signal initiates a series of time-sliced scattering-data acquisitions. This stopped-flow mixer is also equipped with optical paths to monitor absorption or fluorescence from the protein solution in the observation cell.

quality beryllium has also been used. The windows must be thin enough to transmit X-ray photons, but rigid enough to keep a constant beam-path length through sample solutions. A valuable comparison of window materials has been published recently (Henderson, 1995). A protein solution scattering pattern and a corresponding blank scattering curve should be measured in the same sample cell, unless the cells and windows are identical.

Special sample-handling devices have been built for time-resolved studies. Stopped-flow mixers for solution X-ray scattering are routinely used by a number of research groups (Kihara, 1994), and a high-pressure solution cell has been constructed (Czeslik *et al.*, 1996). The assembly process of tobacco mosaic virus has been studied using a temperature-jump apparatus (Hiragi *et al.*, 1988).

19.3.3.3.3. *Designing experiments*

The angular range for data collection should first be determined on the basis of the structural information required, and an instrument should be configured accordingly. Most camera systems have the flexibility to use more than one sample-to-detector distance, and they are occasionally equipped with an additional detector to cover higher angles.

The exposure time is usually determined empirically, taking into account the data statistics required, the number of conditions to be investigated and the total amount of beam time available. Typical exposure times run from a few minutes with a synchrotron source to several hours with a laboratory source. Exposure time depends strongly on the sample molecular weight, the concentration and the angular scattering range of interest. It is essential to measure the blank solvent, *i.e.*, the buffer solution in which the protein of interest is dissolved. It should be recorded with the same statistical significance as the protein solution scattering. This blank is subtracted from the observed protein solution scattering intensity, and therefore its intensity contributes to the overall counting statistics. Accurate blank measurements can take significant amounts of time and should not be ignored when planning the experiment. Blank solution scattering patterns should be recorded as often as possible. They serve as an internal control to detect systematic errors during periods of instrumental instability. In addition, the intensity of the incident X-ray beam should be integrated during the exposure time and used to scale the scattering data. Although it is useful to record the beam intensity transmitted through the solution sample, absorption is generally not a significant problem for solution scattering.

19.3.3.3.4. *Data-collection practices*

Scattering intensity measurements should be performed with a series of experiments. Solutions at different concentrations will demonstrate that the anticipated trends are observed at a qualitative level, even before the data are processed. Time-dependent aggregation or degradation are detected by recording scattering curves in a series, with a short exposure for each curve (*e.g.*, recording 10 successive scattering curves every 30 s for one protein solution). Proteins in solution may degrade in the full flux of a synchrotron-radiation beam and may exhibit radiation-induced aggregation. This is easily recognized by inspecting the very small angle region of scattering patterns that are recorded successively using short exposure times. Radiation damage can be reduced or eliminated either by attenuating the primary beam or by adding small amounts of antioxidants, which may help remove free radicals. There are several cases in which a small amount of dithiothreitol or β-mercaptoethanol prevented radiation-induced aggregation. The effects of the sulfur-reducing agents are consistent with the observation by a time-resolved single-crystal study that the sulfur atom disappears first from an electron-density map (Weik *et al.*, 2000). Temperature control is essential for most experiments. Irradiation by a 9 keV X-ray beam at a rate of 10^{11} photons s^{-1} will heat up an aqueous solution of a few µl by a fraction of a Kelvin per second if a constant-temperature device is not employed.

Preliminary data processing should take place immediately with each sample measurement. Processing 'on the fly' is particularly important when experiments are performed at a synchrotron where access may be limited. Visual inspections or statistical evaluation should be made for time-dependent aggregation at a low scattering angle. A determination of the sample molecular weight by estimating $I(0)$ and the radius of gyration from the Guinier plot would also be useful. In addition to making measurements with a blank, scattering from a standard sample should be measured, allowing the relative molecular weight of the unknown to be determined. A standard, stable, well defined known sample should be recorded prior to any other measurements. Running the same standard sample in every data-collection period makes it easier to compare and scale data sets recorded at different times. Sample solutions should be recovered from sample cells and stored separately, so that post-irradiation concentrations can be measured, as well as their biological activity if this can be assayed. A standard sample that gives sharp diffraction peaks of known spacing should be measured to allow the conversion of the detector channel number to Q values. A dried collagen fibre or a non-biological or more stable specimen such as cholesterol myristate is commonly used. Determining the direct beam position at the detector plane is critical in converting a detector pixel number to a Q value. The symmetric centre of a diffraction pattern of a powder or fibre sample may be used, or a thick metal foil may be inserted to attenuate the primary beam intensity and the beam position measured directly with the detector. In order to place the scattering intensity on an absolute scale, *i.e.*, to determine the scattering cross section, data from a calibrated standard sample need to be recorded.

19.3.3.3.5. *Data processing and analysis*

Processing the solution scattering data first requires scaling the raw intensity measurements to the incident or transmitted beam flux, then averaging scattering curves recorded from identical samples and subtracting measurements from the blanks described above. Corrections for detector non-uniformity or image distortion, if any, must be made, and then the detector channel numbers are converted to Q values (or inverse Bragg-scattering spacing) through the use of the scattering standard for absolute scattering-angle determination. Many facilities provide data-processing support at least to this level. Except for the image-distortion correction, commercially available analysis and visualization software can be used for this purpose. Data formats currently vary among facilities and depend on the detector systems used, but efforts are underway to establish a standard format that would enable the wide use of common data-reduction software. Common formats will make it straightforward to perform data reduction 'on the fly' and to monitor the quality of the data closely. Unfortunately, the size of the biological small-angle scattering community is not conducive to costly development of commercial software, so user friendliness has not generally been a priority in its development.

Plots of I *versus* Q that are corrected for all the known experimental factors are obtained from the data processing, and structural parameters may be derived from these data. The molecular weight and the radius of gyration can be derived immediately from the Guinier approximation. Calculation of the optimal electron pair distribution function by computing the Fourier transform of the intensity function provides the only 'real-space' data directly obtainable from the experiment. The program *GNOM* developed by D. Svergun is widely used for this purpose and may be obtained from the program author. An algorithm developed by P. Moore has been widely implemented, and software developed by

Table 19.3.3.1. *List of commonly used software for solution scattering*

Program	Function	Reference
*OTOKO**	Data evaluation for noncrystalline diffraction	Koch (1988)
SAPOKO	Data evaluation for solution scattering	Koch & Svergun (1992)
GNOM	Indirect Fourier transform for $P(\mathbf{r})$	Svergun (1992)
IFT	Indirect Fourier transform for $P(\mathbf{r})$	Glatter (1999)
CRYSOL	Calculation of $I(Q)$ from PDB files	Svergun *et al.* (1995)
SASHA	Spherical harmonics structure determination	Svergun, Volkov *et al.* (1997)
ASSA and *ALM22INT*	Three-dimensional modelling in real space	Kozin *et al.* (1997)
DAMMIN	Simulated annealing structure determination	Svergun (1999)
DALAI_GA	Genetic algorithm structure determination	Chacón *et al.* (1998)

* An X-terminal compatible version of *OTOKO* has been developed at Daresbury Laboratory.

Glatter *et al.* (Glatter, 1999) is available. Table 19.3.3.1 lists software suites frequently used in interpreting solution X-ray scattering data.

19.3.3.4. *Recent applications of solution X-ray scattering in structural molecular biology*

Solution X-ray scattering provides a direct means of measuring shape at low resolution, *i.e.*, the radius of gyration, the maximum dimension within a protein and the relative molecular weight. Determining the oligomeric state of a protein system is straightforward. Dimensional parameters for simple objects can be obtained indirectly by fitting the observed pattern with spherical or higher-symmetry harmonics. The concept can be extended by use of partial structural models obtained by crystallography and NMR to construct a low-resolution model of large macromolecular complexes that are not amenable to these high-resolution techniques. The refinement of such models against the solution scattering data of the putative complex bridges between atomic resolution structures and biological functions performed by large complexes. Time-resolved studies expand knowledge derived by a variety of structural techniques into the context of experimental molecular dynamics. The examples given below demonstrate some such complementing aspects of solution X-ray scattering studies.

19.3.3.4.1. *Studies of proteins in solution that complement high-resolution structures*

Recent advances in solution scattering data interpretation have made it possible to determine three-dimensional structures at resolutions comparable to those of electron microscopy. In some cases, low-resolution structures were derived from solution X-ray scattering independent of a structural model obtained by other structural techniques. Svergun *et al.* (1994) derived a 15 Å-resolution model of 50S ribosome using the spherical harmonics method. The low-resolution structures of the dimeric and tetrameric forms of pyruvate decarboxylase were obtained by the same method from X-ray solution scattering data (König *et al.*, 1992) before the crystal structure was published. The X-ray structure, at a comparable resolution, was in close agreement with the solution scattering result. The same enzyme obtained from different organisms has also been modelled with solution scattering data.

Calcium-binding proteins have been extensively studied by solution X-ray scattering. These data first demonstrated the large conformation change of calmodulin promoted by binding Ca^{2+} (Seaton *et al.*, 1985). Comparison of the solution scattering curve calculated for the crystal structure of calmodulin with the experimental scattering curve showed that crystal-packing forces substantially altered the solution conformation of the protein (Heidorn & Trewhella, 1988). Kataoka *et al.* (1989) reported the first glimpse of the conformational change of calmodulin induced by melittin, a model peptide for target enzymes. These early studies led to a number of important solution scattering studies on the protein–protein interaction in Ca^{2+}-regulated molecular switching, including the troponin system in muscle contraction. Krueger *et al.* (1997) recently took a combined approach to X-ray and neutron small-angle scattering by using contrast variation to obtain the first structural model of calmodulin complexed with an enzymatically active truncation mutant of skeletal muscle myosin light chain kinase.

A series of structural studies on 70 kDa heat-shock cognate protein, a molecular chaperone, combined crystallography and X-ray solution scattering. It was not possible to crystallize the whole protein, but the crystal structure of the ATPase domain was solved. ATP binding induces a conformational change in the protein, resulting in the release of a bound peptide. Wilbanks *et al.* (1995) constructed a low-resolution model of the whole molecule from solution X-ray scattering data, based on the ATPase domain crystal structure. Solution X-ray scattering was recently used to screen a point-mutated version of the protein, which retains the ATP-induced conformational change, contributing to the interpretation of the role of specific residues in the molecular chaperone mechanism (Sousa & McKay, 1998).

Solution scattering complemented high-resolution NMR structural studies in the investigation of titin (connectin), a giant muscle protein (Improta *et al.*, 1998). The high-resolution structures were determined for two immunoglobulin-like fragments of the I-band region of titin. Two ellipsoids that simulate the molecular envelopes of the two fragments were then used to model solution X-ray scattering data in order to determine the relative position of the two fragments. The resulting structural model suggests that the motions around the interdomain-connecting regions are restricted and that titin behaves as a row of beads connected by rigid hinges. A similar approach was taken for EGF domains in coagulation factor X (Sunnerhagen *et al.*, 1996).

There is a long list of large proteins or protein complexes whose solution X-ray scattering studies have made important contributions in structural biology. One study demonstrated that the quaternary structure of an allosteric enzyme, *E. coli* aspartate transcarbamoylase, in the R (relaxed) state is significantly different from that observed in the R-state crystal, suggesting that a crystal lattice could deform functional quaternary structure (Svergun, Barberato *et al.*, 1997). *A. vinelandii* nitrogenase, the key enzyme in nitrogen fixation, is composed of two proteins: Fe protein and MoFe protein, which were crystallized separately. Grossman *et al.* (1997) determined a low-resolution structure of the complex of Fe and MoFe proteins stabilized by ADP–AlF^{4-}, a nucleotide triphosphate

analogue, solely from solution X-ray scattering data. This was later confirmed by a crystallographic study of the same complex (Schindelin *et al.*, 1997). A more advanced approach was used to construct the three-dimensional structure of *E. coli* F_1 ATPase, which consists of four different soluble subunits in the form of $\alpha_3\beta_3\varepsilon\delta$ (Svergun, Konrad *et al.*, 1998). Two smaller subunits, ε and δ, were disordered in the crystal structure, while NMR provided solution structures for these subunits. Solution scattering was used to construct the three-dimensional structure of the F_1 ATPase structure that incorporates all the subunits. The program *CRYSOL* was used to calculate individual scattering amplitudes by approximating high-resolution structures with sums of spherical harmonics. Then individual amplitudes were combined, according to the relative positions of all subunits, while the subunits were moved with respect to each other to fit the experimental scattering amplitudes obtained for the whole complex. The programs *ASSA* and *ALM22INT* were used to construct the most plausible model for the complex. A 32 Å-resolution structure of *M. Sextra* V_1 ATPase was determined *ab initio* using the spherical harmonics method (Svergun, Aldag *et al.*, 1998). Here, a three-fold molecular symmetry in the A_3B_3 part, which resembles $\alpha_3\beta_3$ in F_1 ATPase, reduced the number of parameters. The model structure of V_1 ATPase has a 110 Å-long stalk region, corresponding to the total mass of the $CDEFG_3$ part of the complex that connects V_1 to the V_0 domain embedded in the membrane.

X-ray scattering amplitudes have recently been used in the correction of the contrast-transfer function in cryo-electron microscopy in an attempt to improve the fidelity of reconstructed electron-microscope models (Thuman-Commike *et al.*, 1999). A low-resolution structure model derived from solution X-ray scattering and electron microscopy was used to obtain initial phases for determining the crystal structure of *E. coli* ClpP, a molecular chaperone (Wang *et al.*, 1997).

19.3.3.4.2. *Time-resolved studies*

The advent of synchrotron-radiation sources made time-resolved X-ray studies of biological macromolecular systems possible. Time-resolved small-angle scattering studies on noncrystalline systems, such as skeletal muscle fibres and proteins in solution, are among the first studies of this type. There is still no other structural technique that offers the means of studying large, real-time conformational changes of macromolecular complexes that cannot be contained within a crystal lattice. This aspect of time-resolved solution scattering thus complements time-resolved Laue crystallography. Arguably, the most important contribution of small-angle solution scattering in recent years is the study of temporal changes in biological molecules resulting from changes in the solution environment. These changes are frequently induced by rapid mixing using a stopped-flow apparatus or a temperature jump that allows a virtually synchronous initiation of a reaction, so that the data reflect a common state for the vast majority of the molecules in solution. The changes may be associations, dissociations [*e.g.* the self-assembly of tobacco mosaic virus (Potschka *et al.*, 1988) and microtubule assembly and oscillation behaviours (Mandelkow *et al.* 1989)], as well as changes in quaternary structure. In time-resolved studies of the allosteric transition of *E. coli* aspartate transcarbamoylase (Tsuruta *et al.*, 1994), a structural intermediate during the enzyme reaction that differs from representative T and R quaternary structures was sought. As the technique has matured, a number of challenging studies have recently been conducted. Many of these time-resolved studies are focused on protein folding, as mentioned below.

19.3.3.4.3. *Protein-folding studies*

There have been a number of solution X-ray scattering studies on protein folding in recent years, in which proteins of low molecular weight had to be investigated under low electron-density contrast due to the presence of denaturing agents, such as urea, at high concentration. Solution X-ray scattering complements other structural techniques used in protein-folding studies, as this is the only technique available for learning how compact a protein is in solution. A Kratky plot of solution scattering data serves as a quick means of determining whether a protein is folded or unfolded. Recently, the singular value decomposition method was applied to this class of problems and revealed a folding intermediate of lysozyme (Chen *et al.*, 1996). This study has recently been expanded to a time-resolved study, which revealed a compact folding intermediate that has not yet formed a hydrophobic core (Chen *et al.*, 1998). Similar studies are being carried out on other protein systems. Arai *et al.* (1998) reported that β-lactoglobulin undergoes a similar folding pattern while it forms a folding intermediate with a hydrophobic core within 100 ms. Uversky *et al.* (1998) reported association-induced folding of globular proteins. Pollack *et al.* (1999) developed a micro-machined mixer to study folding of cytochrome *c* in the sub-millisecond regime.

19.2 (*cont.*)

Auer, M., Scarborough, G. A. & Kühlbrandt, W. (1998). *Three-dimensional map of the plasma membrane H^+-ATPase in the open conformation*. *Nature (London)*, **392**, 840–843.

Baldwin, J. & Henderson, R. (1984). *Measurement and evaluation of electron diffraction patterns from two-dimensional crystals*. *Ultramicroscopy*, **14**, 319–336.

Booy, F. P. & Pawley, J. B. (1993). *Cryo-crinkling: what happens to carbon films on copper grids at low temperature*. *Ultramicroscopy*, **48**, 273–280.

Brink, J. & Chiu, W. (1991). *Contrast analysis of cryo-images of n-paraffin recorded at 400 kV out to 2.1 Å resolution*. *J. Microsc.* **161**, 279–295.

Brink, J. & Chiu, W. (1994). *Applications of a slow-scan CCD camera in protein electron crystallography*. *J. Struct. Biol.* **113**, 23–34.

Brink, J., Gross, H., Tittmann, P., Sherman, M. B. & Chiu, W. (1998). *Reduction of charging in protein electron cryomicroscopy*. *J. Microsc.* **191**, 67–73.

Brink, J., Sherman, M. B., Berriman, J. & Chiu, W. (1998). *Evaluation of charging on macromolecules in electron cryomicroscopy*. *Ultramicroscopy*, **72**, 41–52.

Brink, J. & Wei Tam, M. (1996). *Processing of electron diffraction patterns acquired on a slow-scan CCD camera*. *J. Struct. Biol.* **116**, 144–149.

Butt, H. J., Wang, D. N., Hansma, P. K. & Kühlbrandt, W. (1991). *Effect of surface roughness of carbon support films on high-resolution electron diffraction of two-dimensional protein crystals*. *Ultramicroscopy*, **36**, 307–318.

Chiu, W. & Glaeser, R. M. (1977). *Factors affecting high resolution fixed-beam transmission electron microscopy*. *Ultramicroscopy*, **2**, 207–217.

Chiu, W., Knapek, E., Jeng, T. W. & Dietrick, I. (1981). *Electron radiation damage of a thin protein crystal at 4 K*. *Ultramicroscopy*, **6**, 291–296.

DeRosier, D. J. & Klug, A. (1968). *Reconstruction of three-dimensional structures from electron micrographs*. *Nature (London)*, **217**, 130–134.

Downing, K. H. & Jontes, J. (1992). *Projection map of tubulin in zinc-induced sheets at 4 Å resolution*. *J. Struct. Biol.* **109**, 152–159.

Dubochet, J., Adrian, M., Chang, J.-J., Homo, J.-C., Lepault, J., McDowall, A. W. & Schultz, P. (1988). *Cryo-electron microscopy of vitrified specimens*. *Q. Rev. Biophys.* **21**, 129–228.

Erickson, H. P. & Klug, A. (1970). *The Fourier transform of an electron micrograph: effects of defocusing and aberrations, and implications for the use of underfocus contrast enhancement*. *Philos. Trans. R. Soc. London Ser. B*, **261**, 105–118.

Glaeser, R. M. (1971). *Limitations to significant information in biological electron microscopy as a result of radiation damage*. *J. Ultrastruct. Res.* **36**, 466–482.

Glaeser, R. M. (1992). *Specimen flatness of thin crystalline arrays: influence of the substrate*. *Ultramicroscopy*, **46**, 33–43.

Grigorieff, N., Ceska, T. A., Downing, K. H., Baldwin, J. M. & Henderson, R. (1996). *Electron-crystallographic refinement of the structure of bacteriorhodopsin*. *J. Mol. Biol.* **259**, 393–421.

Hayward, S. B. & Glaeser, R. M. (1979). *Radiation damage of purple membrane at low temperature*. *Ultramicroscopy*, **4**, 201–210.

Henderson, R., Baldwin, J. M., Ceska, T. A., Zemlin, F., Beckmann, E. & Downing, K. H. (1990). *Model for the structure of bacteriorhodopsin based on high-resolution electron cryo-microscopy*. *J. Mol. Biol.* **213**, 899–929.

Henderson, R., Baldwin, J. M., Downing, K. H., Lepault, J. & Zemlin, F. (1986). *Structure of purple membrane from Halobacterium halobium: recording, measurement and evaluation of electron micrographs at 3.5 Å resolution*. *Ultramicroscopy*, **19**, 147–178.

Henderson, R. & Glaeser, R. M. (1985). *Quantitative analysis of image contrast in electron micrographs of beam-sensitive crystals*. *Ultramicroscopy*, **16**, 139–150.

Henderson, R. & Unwin, P. N. (1975). *Three-dimensional model of purple membrane obtained by electron microscopy*. *Nature (London)*, **257**, 28–32.

Hirsch, P., Howie, A., Nicholson, R. B., Pashley, D. W. & Whelan, M. J. (1977). *Electron microscopy of thin crystals*. Huntington: Robert K. Krieger Publishing Co.

Isaacson, M. S. (1977). *Specimen damage in the electron microscope*. In *Principles and techniques of electron micrsocopy. Biological applications*, edited by M. A. Hyatt, pp. 1–78. New York: Van Nostrand Reinhold Co.

Kimura, Y., Vassylyev, D. G., Miyazawa, A., Kidera, A., Matsushima, M., Mitsuoka, K., Murata, K., Hirai, T. & Fujiyoshi, Y. (1997). *Surface of bacteriorhodopsin revealed by high-resolution electron crystallography*. *Nature (London)*, **389**, 206–211.

Kühlbrandt, W., Wang, D. N. & Fujiyoshi, Y. (1994). *Atomic model of plant light-harvesting complex by electron crystallography*. *Nature (London)*, **367**, 614–621.

Mitsuoka, K., Hirai, T., Murata, K., Miyazawa, A., Kidera, A., Kimura, Y. & Fujiyoshi, Y. (1999). *The structure of bacteriorhodopsin at 3.0 Å resolution based on electron crystallography: implication of the charge distribution*. *J. Mol. Biol.* **286**, 861–882.

Miyazawa, A., Fujiyoshi, Y., Stowell, M. & Unwin, N. (1999). *Nicotinic acetylcholine receptor at 4.6 Å resolution: transverse tunnels in the channel wall*. *J. Mol. Biol.* **288**, 765–786.

Nogales, E., Wolf, S. G. & Downing, K. H. (1998). *Structure of the alpha beta tubulin dimer by electron crystallography*. *Nature (London)*, **391**, 199–203.

Prasad, B. V., Degn, L. L., Jeng, T. W. & Chiu, W. (1990). *Estimation of allowable errors for tilt parameter determination in protein electron crystallography*. *Ultramicroscopy*, **33**, 281–285.

Shaw, P. J. & Hills, G. J. (1981). *Tilted specimen in the electron microscope: a simple specimen holder and the calculation of tilt angles for crystalline specimens*. *Micron*, **12**, 279–282.

Sherman, M. B., Brink, J. & Chiu, W. (1996). *Performance of a slow-scan CCD camera for macromolecular imaging in a 400 kV electron cryomicroscope*. *Micron*, **27**, 129–139.

Thomas, I. M. & Schmid, M. F. (1995). *A cross-correlation method for merging electron crystallographic image data*. *J. Micros. Soc. Am.* **1**, 167–173.

Unger, V. M., Kumar, N. M., Gilula, N. B. & Yeager, M. (1999). *Three-dimensional structure of a recombinant gap junction membrane channel*. *Science*, **283**, 1176–1180.

Unwin, P. N. & Henderson, R. (1975). *Molecular structure determination by electron microscopy of unstained crystalline specimens*. *J. Mol. Biol.* **94**, 425–440.

Walz, T., Hirai, T., Murata, K., Heymann, J. B., Mitsuoka, K., Fujiyoshi, Y., Smith, B. L., Agre, P. & Engel, A. (1997). *The three-dimensional structure of aquaporin-1*. *Nature (London)*, **387**, 624–627.

Zhang, P., Toyoshima, C., Yonekura, K., Green, N. M. & Stokes, D. L. (1998). *Structure of the calcium pump from sarcoplasmic reticulum at 8-Å resolution*. *Nature (London)*, **392**, 835–839.

Zhou, Z. H. & Chiu, W. (1993). *Prospects for using an IVEM with a FEG for imaging macromolecules towards atomic resolution*. *Ultramicroscopy*, **49**, 407–416.

19.3

Arai, M., Ikura, T., Semisotnov, G. V., Kihara, H., Amemiya, Y. & Kuwajima, K. (1998). *Kinetic refolding of β-lactoglobulin. Studies by synchrotron X-ray scattering, and circular dichroism, absorption and fluorescence spectroscopy*. *J. Mol. Biol.* **275**, 149–162.

Bonneté, F., Malfois, M., Finet, S., Tardieu, A., Lafont, S. & Veesler, S. (1997). *Different tools to study interaction potentials in γ-crystallin solutions: relevance to crystal growth*. *Acta Cryst.* D**53**, 438–447.

Boulin, C. J., Kempf, A., Gabriel, A. & Koch, M. H. J. (1988). *Data acquisition systems for linear and area X-ray detectors using delay line readout*. *Nucl. Instrum. Methods Phys. Res. A*, **269**, 312–320.

19.3 (*cont.*)

Bu, Z., Perlo, A., Johnson, G. E., Olack, G., Engelman, D. M. & Wyckoff, H. W. (1998). *A small-angle X-ray scattering apparatus for studying biological macromolecules in solution*. *J. Appl. Cryst.* **31**, 533–543.

Chacón, P., Morán, F., Díaz, J. F., Pantos, E. & Andreu, J. M. (1998). *Low-resolution structures of proteins in solution retrieved from X-ray scattering with a genetic algorithm*. *Biophys. J.* **74**, 2760–2775.

Chen, L., Hodgson, K. O. & Doniach, S. (1996). *A lysozyme folding intermediate revealed by solution X-ray scattering*. *J. Mol. Biol.* **261**, 658–671.

Chen, L., Wildegger, G., Kiefhaber, T., Hodgson, K. O. & Doniach, S. (1998). *Kinetics of lysozyme refolding: structural characterization of a non-specifically collapsed state using time-resolved X-ray scattering*. *J. Mol. Biol.* **276**, 225–237.

Cipriani, F., Gabriel, A. & Koch, M. H. J. (1994). *Alternative approaches to delay line readout for multiwire proportional chambers*. *Nucl. Instrum. Methods A*, **346**, 286–291.

Czeslik, C., Malessa, R., Winter, R. & Rapp, G. (1996). *High pressure synchrotron X-ray diffraction studies of biological molecules using the diamond anvil technique*. *Nucl. Instrum. Methods Phys. Res. A*, **368**, 847–851.

Dubuisson, J.-M., Decamps, T. & Vachette, P. (1997). *Improved signal-to-background ratio in small-angle X-ray scattering experiments with synchrotron radiation using an evacuated cell for solutions*. *J. Appl. Cryst.* **30**, 49–54.

Feigin, L. A. & Svergun, D. I. (1987). *Structure analysis by small-angle X-ray and neutron scattering*. New York: Plenum Press.

Genick, U., Borgstahl, G. E. O., Ng, K., Ren, Z., Pradervand, C., Burke, P. M., Srajer, V., Teng, T.-Y., Schildkamp, W., McRee, D. E., Moffat, K. & Getzoff, E. D. (1997). *Structure of a protein photocycle intermediate by millisecond time-resolved crystallography*. *Science*, **275**, 1471–1475.

Glatter, O. (1999). *X-ray techniques*. In *International tables for crystallography*, Vol. C. *Mathematical, physical and chemical tables*, edited by A. J. C. Wilson & E. Prince, pp. 89–104. Dordrecht: Kluwer Academic Publishers.

Glatter, O. & Kratky, O. (1982). Editors. *Small angle X-ray scattering*. London: Academic Press.

Griffith, J. P., Griffith, D. L., Rayment, I., Murakami, W. T. & Caspar, D. L. D. (1992). *Inside polyomavirus at 25-Å resolution*. *Nature (London)*, **355**, 652–654.

Grossman, J. G., Hasnain, S. S., Yousafzai, F. K., Smith, B. E. & Eady, R. R. (1997). *The first glimpse of a complex of nitrogenase component proteins by solution X-ray scattering: conformation of the electron transfer transition state complex of Klebsiella pneumonia nitrogenase*. *J. Mol. Biol.* **266**, 642–648.

Guinier, A. & Fournet, G. (1955). *Small-angle scattering of X-rays*. New York: John Wiley & Sons.

Harrison, S. C. (1969). *Structure of tomato bushy stunt virus. I. The spherically averaged electron density*. *J. Mol. Biol.* **42**, 457–483.

Heidorn, D. B. & Trewhella, J. (1988). *Comparison of the crystal and solution structures of calmodulin and troponin C*. *Biochemistry*, **27**, 909–915.

Henderson, S. J. (1995). *Comparison of parasitic scattering from window materials used for small-angle X-ray scattering: a better beryllium window*. *J. Appl. Cryst.* **28**, 820–826.

Hiragi, Y., Nakatani, H., Kajiwara, K., Inoue, H., Sano, Y. & Kataoka, M. (1988). *Temperature-jump apparatus and measuring system for synchrotron solution X-ray scattering experiments*. *Rev. Sci. Instrum.* **59**, 64–66.

Improta, S., Krueger, J. K., Gautel, M., Atkinson, R. A., Lefevre, J. F., Moulton, S., Trewhella, J. & Pastore, A. (1998). *The assembly of immunoglobulin-like modules in titin: implications for muscle elasticity*. *J Mol. Biol.* **284**, 761–777.

Inouye, H., Tsuruta, H., Sedzik, J., Uyemura, K. & Kirschner, D. A. (1999). *Tetrameric assembly of full-sequence protein zero myelin glycoprotein by synchrotron X-ray scattering*. *Biophys. J.* **76**, 423–437.

Jack, A. & Harrison, S. C. (1975). *On the interpretation of small-angle X-ray solution scattering from spherical viruses*. *J. Mol. Biol.* **99**, 15–25.

Johnson, J. E. & Hollingshead, C. (1981). *Crystallographic studies of cowpea mosaic virus by electron microscopy and X-ray diffraction*. *J. Ultrastruct. Res.* **74**, 223–231.

Kataoka, M., Head, J. F., Seaton, B. A. & Engelman, D. M. (1989). *Melittin binding causes a large calcium-dependent conformational change in calmodulin*. *Proc. Natl Acad. Sci. USA*, **86**, 6944–6948.

Kihara, H. (1994). *Stopped-flow apparatus for X-ray scattering and XAFS*. *J. Synchrotron Rad.* **1**, 74–77.

Koch, M. H. J. (1988). *Instruments and methods for small-angle scattering with synchrotron radiation*. *Makromol. Chem. Macromol. Symp.* **15**, 79–90.

Koch, M. H. J. (1991). *Scattering from non-crystalline systems*. In *Handbook on synchrotron radiation*, Vol. 4, edited by S. Ebashi, M. Koch & E. Rubenstein. Amsterdam: Elsevier Science Publishers.

Koch, M. H. J. & Svergun, D. I. (1992). Unpublished result.

König, S., Svergun, D., Koch, M. H. J., Höbner, G. & Schellenberger, A. (1992). *Synchrotron radiation solution X-ray scattering study of the pH dependence of the quaternary structure of yeast pyruvate decarboxylase*. *Biochemistry*, **31**, 8726–8731.

Kozin, M. B., Volkov, V. V. & Svergun, D. I. (1997). *ASSA, a program for three-dimensional rendering in solution scattering from biopolymers*. *J. Appl. Cryst.* **30**, 811–815.

Krueger, J. K., Glah, G. A., Rokop, S. E., Zhi, G., Stull, J. T. & Trewhella, J. (1997). *Structures of calmodulin and a functional myosin light chain kinase in the activated complex: a neutron scattering study*. *Biochemistry*, **36**, 6017–6023.

Lattman, E. E. (1989). *Rapid calculation of the solution scattering profile from a macromolecule of known structure*. *Protein Struct. Funct. Genet.* **5**, 149–155.

Mandelkow, E., Lange, G. & Mandelkow, E. M. (1989). *Applications of synchrotron radiation to the study of biopolymers in solution time-resolved X-ray scattering of microtubule self-assembly and oscillations*. *Top. Curr. Chem.* **151**, 2–30.

Miller, S. T., Genova, J. D. & Hogle, J. M. (1999). *Collection of very low resolution protein data. J. Appl. Cryst.* **32**, 1183–1185.

Moffat, K. (1997). *Laue diffraction*. *Methods Enzymol.* **277**, 433–447.

Moore, P. B. (1980). *Small-angle scattering. Information content and error analysis*. *J. Appl. Cryst.* **13**, 168–175.

Mourey, L., Pédelacq, J.-D., Fabre, C., Causse, H., Rougé, P. & Samama, J.-P. (1997). *Small-angle X-ray scattering and crystallographic studies of arcelin-1: an insecticidal lectin-like glycoprotein from Phaseolus vulgaris L. Proteins*, **29**, 433–442.

Olah, G. A., Gray, D. M., Gray, C. W., Kergil, D. L., Sosnick, T. R., Mark, B. L., Vaughan, M. R. & Trewhella, J. (1995). *Structures of fd gene 5 protein–nucleic acid complexes: a combined solution scattering and electron microscopy study*. *J. Mol. Biol.* **249**, 576–594.

Petitpas, I., Lepault, J., Vachette, P., Charpilienne, A., Mathieu, M., Kohli, E., Pothier, P., Cohen, J. & Reyl, F. A. (1998). *Crystallization and preliminary X-ray analysis of rotavirus protein VP6*. *J. Virol.* **72**, 7615–7619.

Petrascu, A.-M., Koch, M. H. J. & Gabriel, A. (1998). *A beginners' guide to gas-filled proportional detectors with delay line readout*. *J. Macromol. Sci. Phys.* B**37**, 463–483.

Pilz, I., Glatter, O. & Kratky, O. (1979). *Small-angle X-ray scattering*. *Methods Enzymol.* **61**, 148–249.

Pollack, L., Tate, M. W., Darnton, N. C., Knight, J. B., Gruner, S. M., Eaton, W. A. & Austin, R. H. (1999). *Compactness of the denatured state of a fast-folding protein measured by submillisecond small-angle X-ray scattering. Proc. Natl Acad. Sci. USA*, **96**, 10115–10117.

Potschka, M., Koch, M. H. J., Adams, M. L. & Schuster, T. M. (1988). *Time-resolved solution X-ray scattering of tobacco mosaic virus coat protein: kinetics and structure of intermediates*. *Biochemistry*, **27**, 8481–8491.

Schindelin, H., Kisker, C., Schlessman, J. L., Howard, J. B. & Rees, D. C. (1997). *Structure of ADP. AlF-4-stabilized nitrogenase*

19.3 (*cont.*)

complex and its implications for signal transduction. *Nature (London)*, **387**, 370–376.
Schmidt, T., Johnson, J. E. & Phillips, W. (1983). *The spherically averaged structures of cowpea mosaic virus components by X-ray solution scattering*. *Virology*, **127**, 65–73.
Schuster, M. & Göbel, H. (1995). *Parallel-beam coupling into channel-cut monochromators using curved graded multilayers*. *J. Phys. D*, **28**, A270–A275.
Seaton, B. A., Head, J. F., Engelman, D. M. & Richards, F. M. (1985). *Calcium-induced increase in the radius of gyration and maximum dimension of calmodulin measured by small-angle X-ray scattering*. *Biochemistry*, **24**, 6740–6743.
Sousa, M. C. & McKay, D. B. (1998). *The hydroxyl of threonine 13 of the bovine 70-kDa heat shock cognate protein is essential for transducing the ATP-induced conformational change*. *Biochemistry*, **37**, 15392–15399.
Srajer, V., Teng, T.-Y., Ursby, T., Pradervand, C., Ren, Z., Adachi, S., Bourgeois, D., Wulff, M. & Moffat, K. (1996). *Photolysis of the carbon monoxide complex of myoglobin: nanosecond time-resolved crystallography* [see *Comments*]. *Science*, **274**, 1726.
Stuhrmann, H. B. (1970). *Interpretation of small-angle scattering functions of dilute solutions and gases. A representation of the structures related to a one-particle-scattering function*. *Acta Cryst.* A**26**, 297–306.
Sunnerhagen, M., Olah, G. A., Stenflo, J., Forsen, S., Drakenberg, T. & Trewhella, J. (1996). *The relative orientation of Gla and EGF domains in coagulation factor X is altered by Ca-2+ binding to the first EGF domain. A combined NMR–small angle X-ray scattering study*. *Biochemistry*, **35**, 11547–11559.
Svergun, D. I. (1992). *Determination of the regularization parameter in indirect-transform methods using perceptual criteria*. *J. Appl. Cryst.* **25**, 495–503.
Svergun, D. I. (1999). *Restoring low resolution structure of biological macromolecules from solution scattering using simulated annealing*. *Biophys. J.* **76**, 2879–2886.
Svergun, D. I., Aldag, I., Sieck, T., Altendorf, K., Koch, M. H. J., Kane, D. J., Kozin, M. B. & Grueber, G. (1998). *A model of the quaternary structure of the Escherichia coli F1 ATPase from X-ray solution scattering and evidence for structural changes in the Delta subunit during ATP hydrolysis*. *Biophys. J.* **75**, 2212–2219.
Svergun, D. I., Barberato, C. & Koch, M. H. J. (1995). *CRYSOL – a program to evaluate X-ray solution scattering of biological macromolecules from atomic coordinates*. *J. Appl. Cryst.* **28**, 768–773.
Svergun, D. I., Barberato, C., Koch, M. H. J., Fetler, L. & Vachette, P. (1997). *Large differences are observed between the crystal and solution quaternary structures of allosteric aspartate transcarbamylase in the R state*. *Proteins Struct. Funct. Genet.* **27**, 110–117.
Svergun, D. I., Koch, M. H. & Serdyuk, I. N. (1994). *Structural model of the 50 S subunit of Escherichia coli ribosomes from solution scattering. I. X-ray synchrotron radiation study*. *J. Mol. Biol.* **240**, 66–77.
Svergun, D. I., Konrad, S., Huss, M., Koch, M. H. J., Wieczorek, H., Altendorf, K., Volkov, V. V. & Grueber, G. (1998). *Quaternary structure of V_1 and F_1 ATPase: significance of structural homologies and diversities*. *Biochemistry*, **37**, 17659–17663.
Svergun, D. I., Richard, S., Koch, M. H. J., Sayers, Z., Kuprin, S. & Zaccai, G. (1998). *Protein hydration in solution: experimental observation by X-ray and neutron scattering*. *Proc. Natl Acad. Sci. USA*, **95**, 2267–2272.
Svergun, D. I., Volkov, V. V., Kozin, M. B. & Stuhrmann, H. B. (1996). *New developments in direct shape determination from small-angle scattering. 2. Uniqueness*. *Acta Cryst.* A**52**, 419–426.
Svergun, D. I., Volkov, V. V., Kozin, M. B., Stuhrmann, H. B., Barberato, C. & Koch, M. H. J. (1997). *Shape determination from solution scattering of biopolymers*. *J. Appl. Cryst.* **30**, 798–802.
Thuman-Commike, P. A., Tsuruta, H., Greene, B., Prevelige, P. E., King, J. & Chiu, W. (1999). *Solution X-ray scattering based estimation of electron cryomicroscopy imaging parameters for reconstruction of virus particles*. *Biophys. J.* **76**, 2249–2261.
Trewhella, J. (1998). *Insights into biomolecular function from small-angle scattering*. *Curr. Opin. Struct. Biol.* **7**, 702–708.
Tsuruta, H., Reddy, V., Wikoff, W. & Johnson, J. (1998). *Imaging RNA and dynamic protein segments with low resolution virus crystallography; experimental design, data processing and implications of electron density maps. J. Mol. Biol.* **284**, 1439–1452.
Tsuruta, H., Vachette, P., Sano, T., Moody, M. F., Amemiya, Y., Wakabayashi, K. & Kihara, H. (1994). *Kinetics of the quaternary structure change of aspartate transcarbamylase triggered by succinate, a competitive inhibitor*. *Biochemistry*, **33**, 10007–10012.
Uversky, V. N., Segel, D. J., Doniach, S. & Fink, A. L. (1998). *Association-induced folding of globular proteins*. *Proc. Natl Acad. Sci. USA*, **95**, 5480–5483.
Wang, J., Harting, J. A. & Flanagan, J. M. (1997). *The structure of ClpP at 2.3 Å resolution suggests a model for ATP-dependent proteolysis*. *Cell*, **91**, 447–456.
Weik, M., Ravelli, R. B. G., Kryger, G., McSweeney, S., Raves, M. L., Harel, M., Gros, P., Silman, I., Kroon, J. & Sussman, J. L. (2000). *Specific chemical and structural damage to proteins produced by synchrotron radiation. Proc. Natl Acad. Sci. USA*, **97**, 623–628.
Wikoff, W., Duda, R., Hendrix, R. & Johnson, J. (1998). *Crystallization and preliminary X-ray analysis of the dsDNA bacteriophage HK97 mature empty capsid*. *Virology*, **243**, 113–118.
Wilbanks, S. M., Chen, L., Tsuruta, H., Hodgson, K. O. & McKay, D. B. (1995). *Solution small-angle X-ray scattering study of the molecular chaperone Hsc70 and its subfragments*. *Biochemistry*, **34**, 12095–12106.
Yamashita, M. M., Almassy, R. J., Janson, C. A., Cascio, D. & Eisenberg, D. (1989). *Refined atomic model of glutamine synthetase at 3.5 Å resolution*. *J. Biol. Chem.* **264**, 17681–17690.
Zheng, Y., Doerschuk, P. C. & Johnson, J. E. (1995). *Determination of three-dimensional low-resolution viral structure from solution X-ray scattering data*. *Biophys. J.* **69**, 619–639.

19.4

Atkinson, D. & Shipley, G. G. (1984). *Structural studies of plasma lipoproteins*. *Basic Life Sci.* **27**, 211–226.
Bacon, G. E. (1975). *Neutron diffraction*. Oxford University Press.
Baldwin, J. P., Boseley, P. G., Bradbury, E. M. & Ibel, K. (1975). *The subunit structure of the eukaryotic chromosome*. *Nature (London)*, **253**, 245–249.
Bilgin, N., Ehrenberg, M., Ebel, C., Zaccai, G., Sayers, Z., Koch, M. H. J., Svergun, D. I., Barberato, C., Volkov, V., Nissen, P. & Nyborg, J. (1998). *Solution structure of the ternary complex between aminoacyl-tRNA, elongation factor Tu, and guanosine triphosphate*. *Biochemistry*, **37**, 8163–8172.
Bradbury, E. M., Baldwin, J. P., Carpenter, B. G., Hjelm, R. P., Hancock, R. & Ibel, K. (1976). *Neutron-scattering studies of chromatin*. *Brookhaven Symp Biol.* **27**, IV97–IV117.
Bragg, W. L. & Perutz, M. F. (1952). *The external form of the haemoglobin molecule. I*. *Acta Cryst.* **5**, 277–283.
Burks, C. & Engelman, D. M. (1981). *Cholesteryl myristate conformation in liquid crystalline mesophases determined by neutron scattering*. *Proc. Natl Acad. Sci. USA*, **78**, 6863–6867.
Capel, M. S., Engelman, D. M., Freeborn, B. R., Kjeldgaard, M., Langer, J. A., Ramakrishnan, V., Schindler, D. G., Schneider, D. K., Schoenborn, B. P. & Sillers, I. Y. (1987). *A complete mapping of the proteins in the small ribosomal subunit of Escherichia coli*. *Science*, **238**, 1403–1406.
Crichton, R., Engelman, D. M., Hass, J., Koch, M. H. J., Moore, P. B., Parfait, R. & Stuhrmann, H. B. (1977). *A contrast variation study of specifically deuterated ribosomal subunits*. *Proc. Natl Acad. Sci. USA*, **74**, 5547–5550.
Debye, P. (1915). *Zerstreuung von Röntgenstrahlen. Ann. Phys. (Leipzig)*, **46**, 809–823.